

Atomistic deformation modes and intrinsic brittleness of Al_4SiC_4 : A first-principles investigationTing Liao,^{1,2} Jingyang Wang,^{1,3} and Yanchun Zhou¹¹*Shenyang National Laboratory for Materials Science, Institute of Metal Research,
Chinese Academy of Sciences, Shenyang 110016, China*²*Graduate School of Chinese Academy of Sciences, Beijing 100039, China*³*International Centre for Materials Physics, Institute of Metal Research, Chinese Academy of Sciences, Shenyang 110016, China*

(Received 31 July 2006; revised manuscript received 10 October 2006; published 16 November 2006)

From crystallographic point of view, Al_4SiC_4 can be described as Al_4C_3 -type and hexagonal SiC-type structural units alternatively stacked along [0001] direction. However, relationship between this layered crystal structure and mechanical properties is not fully established for Al_4SiC_4 , except for the reported bulk modulus locating between those of Al_4C_3 and SiC. Based on the first-principles pseudopotential total energy method, we calculated the elastic stiffness of Al_4SiC_4 , and reported on its ideal tensile and shear stress-strain relationships considering different structural deformation modes. Elastic properties of Al_4SiC_4 are dominated by the Al_4C_3 -type structural units and exhibit similar results with those of Al_4C_3 . Furthermore, the atomistic deformation modes of Al_4SiC_4 upon tensile and shear deformations are illustrated and compared with Al_4C_3 as well. Since the tension-induced bond breaking occurs inside the constitutive Al_4C_3 -type unit, the ternary carbide has similar ideal tensile strength with Al_4C_3 . On the other hand, despite the softening of strong coupling between Al_4C_3 - and SiC-type structural units is involved in shear, the shear strength for Al_4SiC_4 is, however, lower than the tensile strength, since p -state involved Al-C bonds respond more readily to the shear deformation than to tension. In addition, based on the comparison of strain energies at the maximum stresses, i.e., ideal strengths, for both tension and shear, we suggest that structural failure occurs in tensile deformation firstly and, thus confirms an intrinsic brittleness of Al_4SiC_4 . For crystal structure arranged in alternatively stacking configuration, such as Al_4SiC_4 , mechanical properties can be traced back to the constituent units, and are also related to the coupling strengths between each constituent unit. The results might provide a computational method to predict ductile or brittle response of a solid to applied deformations.

DOI: [10.1103/PhysRevB.74.174112](https://doi.org/10.1103/PhysRevB.74.174112)

PACS number(s): 81.05.Je, 62.20.-x, 71.20.-b

I. INTRODUCTION

A large number of aluminum-containing ternary ceramics are among the most promising candidates for high temperature structural application and part of them as oxidation-protective multicomposition coatings.¹ Well-documented layered ternary aluminum carbides, such as Ti_3AlC_2 , Ti_2AlC , and Nb_2AlC , have been reported to be hexagonal crystals and have many astonishing properties, such as room temperature ductility, oxidation resistance, and good damage tolerance,² differing dramatically from their binary counterparts. Another group of ternary aluminum carbides in the Zr-Al-C and Hf-Al-C systems were also studied. Among them $\text{Zr}_3\text{Al}_3\text{C}_5$ and $\text{Hf}_3\text{Al}_3\text{C}_5$ were determined to have the hexagonal symmetry too.³ By means of *ab initio* pseudopotential total energy calculations,⁴ $\text{Zr}_3\text{Al}_3\text{C}_5$ was predicted to have similar mechanical properties to the hard binary carbide, ZrC. As a thumb rule, many properties, particularly mechanical properties, could be traced back to the crystal structures.

These layered ternary carbides can be described as various structural units arranged alternatively along the c direction with different coupling strengths. For example, crystal structure of Ti_2AlC or Nb_2AlC is described as Ti_2C or Nb_2C slabs in a NaCl-type structure being intercalated and mirrored by close-packed Al atomic planes, and $\text{Zr}_3\text{Al}_3\text{C}_5$ may be viewed as the nonstoichiometric ZrC_x slabs in NaCl-type structure being coupled to Al_4C_3 -type Al-C layers.⁵ The mechanical properties of these aluminum-containing ternary

carbides are, therefore, determined by the coupling strengths between each structural unit, or the structural unit itself. According to previous theoretical investigations, the machinability, damage tolerance, and microscale ductility of ternary Ti_2AlC and Nb_2AlC phases are totally traceable to the weak coupling between the transition metal carbide units and the planar aluminum atomic layers, while the high bulk modulus and Young's moduli are originated from the strong Ti_2C or Nb_2C slabs.^{6–8} Similarly, bonding strength analysis suggest that the strong coupling of Zr-C blocks to Al-C layers are decisive to the mechanical properties of $\text{Zr}_3\text{Al}_3\text{C}_5$.⁴

Aluminum silicon carbide, Al_4SiC_4 , is another aluminum-containing ternary carbide and has been characterized by low theoretical density, high melting point, high heat conductivity, and excellent oxidation resistance.^{9,10} If fine particles Al_4SiC_4 is dispersed in C/C composites, mullite ($3\text{Al}_2\text{O}_3 \cdot 2\text{SiO}_2$) is expected to be formed directly by their oxidation and hence, an improvement of oxidation resistance is achieved for the C/C composites.¹¹ As illustrated in Fig. 1, Al_4SiC_4 may be viewed as an intergrown structure consisting of two kinds of layers. One is the Al-C slab in an Al_4C_3 -type structure and the other consists of Si and C atoms in an arrangement similar to that in any polytype of silicon carbide, SiC. The Al_4SiC_4 has been widely studied and proved to be excellent in oxidation resistance at high temperature.^{11,12} The bulk modulus was recently reported to be 182 GPa, which locates between those of Al_4C_3 and SiC.¹³ For a structural ceramic with potential high-temperature applications, the correlation between the elec-

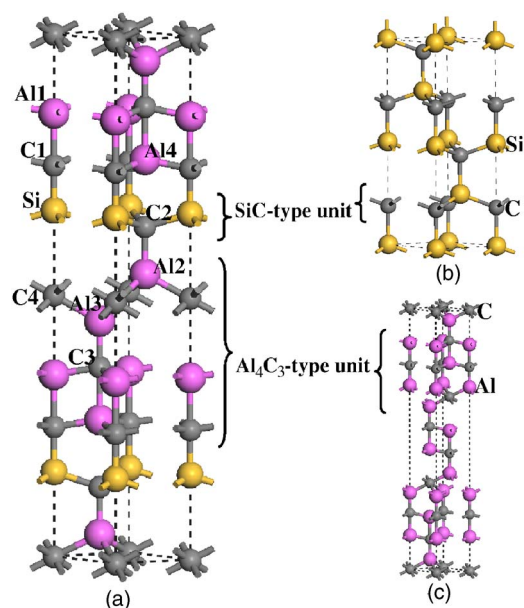


FIG. 1. (Color online) Crystal structures of (a) Al_4SiC_4 , (b) 4H-SiC, and (c) Al_4C_3 . The yellow, purple, and gray balls represent Al, Si, and C atoms, respectively. The Al and C atoms in Al_4SiC_4 are indexed with numbers according to various coordination environments.

tronic structure, crystal structure, and mechanical properties should be fully established for Al_4SiC_4 at first. Analogous to the above mentioned aluminum-containing ternary carbides, it is helpful to clarify how the mechanical properties of Al_4SiC_4 are determined by its intergrown structure or coupling strength between different structural units. Moreover, it is meaningful to generalize current analytic characteristics to further prediction of mechanical properties for other crystals stacked in layered arrangement. In this study, we computed the elastic stiffness, ideal strengths, atomistic deformation modes, and chemical bonding characteristics of Al_4SiC_4 using the first-principles computational scheme. The investigation aims to study possible deformation modes, and further, to show the relationship between the crystal structure and the mechanical properties. The quest for the strain energy comparison at the maximum stresses, i.e., ideal strengths, between shear and tension is also performed to unveil the intrinsic brittleness of Al_4SiC_4 .

Predicting mechanical properties based on first-principles calculation has been frequently focused in the past decades.^{14–17} First-principles study on the stress-strain relation can establish the detailed atomistic bond softening and breaking modes of materials and, thus predict the mechanical responses to applied strains. The calculated elastic constants determine the behavior of material under small deformation when the stress-strain relation is still linear. Another important parameter, which describes the behavior of material near the limit of structural stability, is the ideal strengths. The ideal tensile and shear strengths represent the upper bound stresses necessary for cleavage, slip, or fracture of the crystal. As an inherent property of crystal lattice, the strengths offer insight into the correlation between the intrinsic chemical bonding and mechanical properties.¹⁸ Studies of the

stress-strain relations and the underlying atomistic deformation processes can provide important insights into the fundamental aspects of deformation and failure modes, which are critical to understanding the mechanical properties. Moreover, ductility of a solid is controlled by the energy needed to break bonds by shear compared to that by tension.^{19–21} It has been characterized that Ti_2AlC and Ti_2AlN yield a large ratio of tensile strength to the shear one,²² suggesting an intrinsic ductility. The atomistic deformation modes of TiC and TiN suggest intrinsic brittleness quantitatively represented by comparable tensile to shear ideal strengths. In the present work, we hope to establish an atomistic description of the deformation modes of Al_4SiC_4 to further understand the correlation between structure and its properties.

The remainder of this paper is organized as follows. The computational details are described in Sec. II. In Sec. III, we present results for equilibrium geometry and elastic stiffness of Al_4SiC_4 , together with the full set of elastic coefficients of Al_4C_3 and 4H-SiC for comparison. The ideal stress-strain relationship, ideal tensile, and shear strength, along with the description of atomistic deformation modes for material strained from elasticity to structural instability, are illustrated in Sec. IV. Finally, the concluding remarks are given in Sec. V.

II. COMPUTATIONAL DETAILS

The equilibrium crystal parameters and ground-state electronic structure were calculated using the CASTEP (Ref. 23) code, in which the plane-wave pseudopotential total energy calculation was performed. Interactions of electrons with ion cores were represented by the Vanderbilt-type ultrasoft pseudopotential for Al, Si, and C atoms.²⁴ The electronic exchange-correlation energy was treated under the generalized gradient approximation (GGA-PW91).²⁵ The plane-wave basis set cutoff was set as 450 eV for all cases, which was sufficient in leading to good convergence for total energy and forces acting on the atoms. The special points sampling integration over the Brillouin zone was employed by using the Monkhorst-Pack method with $10 \times 10 \times 2$ special k -point meshes.²⁶ The tolerances for the geometry optimization were selected as the difference in total energy within 5.0×10^{-6} eV/atom, the maximum ionic Hellmann-Feynman force within 0.01 eV/Å, the maximum ionic displacement within 5.0×10^{-4} Å, and the maximum stress within 0.02 GPa. Increasing the plane-wave cutoff energy to 700 eV and the k -point meshes to $14 \times 14 \times 2$ changed the total energy and lattice constants by less than 0.003 eV/atom and 0.004%, respectively. Therefore, the present computations were precise enough to represent the ground state properties of studied compounds. To investigate the bonding strengths of different bonds, the lattice configurations were optimized at various isotropic hydrostatic pressures ranging from 0 to 50 GPa. Lattice parameters, including lattice constants and internal atomic coordinates, were modified independently to minimize the free enthalpy, interatomic forces and unit-cell stresses. The Brodyden-Fletcher-Goldfarb-Shanno (BFGS) minimization scheme²⁷ was used in geometry optimization.

The elastic coefficients were determined from a first-principles calculation by applying a set of given homogeneous deformations with a finite value and calculating the resulting stress with respect to optimizing the internal degrees of freedom, as implemented by Milman *et al.*²⁸ The criteria for convergence in optimizing atomic internal freedoms were selected as follows: difference on total energy within 1×10^{-6} eV/atom, ionic Hellmann-Feynman forces within 0.002 eV/Å and maximum ionic displacement within 1×10^{-4} Å. Two strain patterns, one with nonzero ε_{11} and ε_{23} components and other with a nonzero ε_{33} , generated stresses related to all five independent elastic coefficients for a unit cell with hexagonal symmetry. Three positive and three negative amplitudes were applied for each strain pattern with a maximum strain value of 0.5%. We determined the elastic coefficients from linear fits of calculated stresses as a function of strains. The compliance tensor S was calculated as the inverse of the stiffness tensor, $S=C^{-1}$. Other mechanical parameters, such as bulk modulus, Young's moduli, and Poisson's ratio were calculated from the compliance tensor. The shear modulus was calculated according to the Voigt approximation.²⁹

Investigation of the atomistic deformation modes was performed by straining material far beyond the elastic region. We applied a series of incremental strains to the unit cell under constant-strain-constraint condition, along the 0001, $[1\bar{2}10](0001)$, and $[\bar{1}010](0001)$ strain paths, respectively, and calculated the achieved tensile and shear stresses. To ensure that the unit cell was under a uniaxial stress condition, we relaxed all other degrees of freedom (including cell constants and internal atomic coordinates) until the calculated Hellmann-Feynman stresses are less than 0.2 GPa, with constraining the applied strain. The first maximum in stress-strain curve is regarded as the ideal strength.

III. EQUILIBRIUM GEOMETRY AND ELASTIC STIFFNESS

The equilibrium crystal structure of Al_4SiC_4 belongs to the $P6_3mc$ space group and is proposed as being similar to that of aluminum carbonitride $\text{Al}_4\text{C}_3\text{N}$. The crystal structure of Al_4SiC_4 is illustrated in Fig. 1 and, the Al and C atoms are indexed with various numbers according to different coordination environments. Silicon atoms are located at $2a$ Wyck-off positions. Aluminum and carbon atoms both occupy four structurally nonequivalent positions: Al atoms have three in $2b$ and one in $2a$ Wyckoff positions, and C atoms have two in $2a$ and two in $2b$ positions, respectively. For comparison, the crystal structures of Al_4C_3 and 4H-SiC are also plotted. The hexagonal 4H-SiC has the smallest unit cell that contains inequivalent atomic sites with either cubic (k) or hexagonal (h) character in the complex SiC polytypes. As can be seen from Fig. 1, the structural relationships between Al_4SiC_4 , Al_4C_3 , and hexagonal polytype 4H-SiC are well stated. The crystal structure of Al_4SiC_4 can be described as an intergrown structure consisting of two kinds of layers stacking alternately along the $[0001]$ direction. One is composed of Al and C atoms in an arrangement resembling the binary aluminum carbide, Al_4C_3 , and the other is corner-

TABLE I. Theoretical and experimental lattice parameters (in Å) and c/a ratio of Al_4SiC_4 , Al_4C_3 , and 4H-SiC.

	Method	a	c	c/a
Al_4SiC_4	Calc.	3.222	21.352	6.627
	Expt. ^a	3.277	21.74	6.634
Al_4C_3	Calc.	3.281	24.547	7.482
	Expt. ^b	3.331	24.99	7.502
4H-SiC	Calc.	3.036	9.936	3.273
	Expt. ^c	3.081	10.085	3.273

^aReference 13.

^bReference 30.

^cReference 31.

sharing SiC_4 tetrahedra derived from any polytype of SiC crystal structures. Coupling between the Al_4C_3 - and SiC-type structural units may also play a key role for the mechanical properties and structural stability of Al_4SiC_4 . Theoretical lattice parameters of Al_4SiC_4 , Al_4C_3 , and 4H-SiC are listed in Table I, together with the experimental values for comparison.^{13,30,31} The computed lattice constants a and c of studied compounds are in consistency with experimental data within 2% deviation. Therefore, the present first-principles computation is reliable to reproduce the equilibrium crystal structures of the compounds.

To illustrate the bonding strengths in Al_4SiC_4 , we present the bond-length contractions under various hydrostatic pressures in Fig. 2, together with the axial ratio, c/a , as a function of external pressure plotted in the inset. As shown in Fig. 2, the highest lying curve associates with the Si-C1 bond and shows the most resistive character to applied pressure among the illustrated bonds. The Si-C1 bond corresponds to the coupling between the Al_4C_3 - and SiC-type structural units, which implies that an enhanced mechanical property might be achieved for Al_4SiC_4 compared with that of Al_4C_3 . The lowest lying curve shows the most compressible feature and corresponds to Al1-C1 bond along the c direction. Since the Al1-C1 bonds locate in the Al_4C_3 -type structural unit, Al_4SiC_4 is expected to be in more resemblance in mechanical properties with the binary carbide, Al_4C_3 , because of the

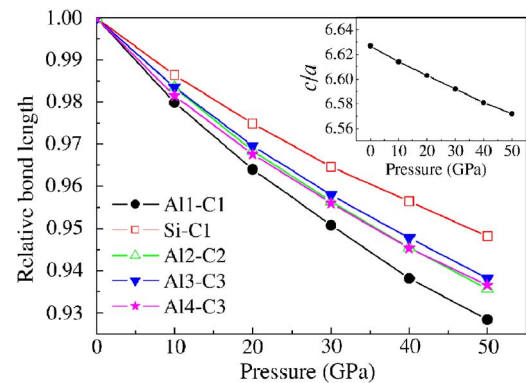


FIG. 2. (Color online) Bond-length contractions in Al_4SiC_4 under various pressures, together with the axial ratio c/a as a function of pressure shown in the inset.

TABLE II. Calculated second order elastic constants c_{ij} (in GPa) for Al_4SiC_4 , Al_4C_3 , and 4H-SiC .

Compound	c_{11}	c_{12}	c_{13}	c_{33}	c_{44}	c_{66}
Al_4SiC_4	386	118	50	409	122	134
Al_4C_3	352	115	52	391	116	119
4H-SiC	532	102	48	577	175	215

weakest bonding. The other three curves, associated with Al2-C2, Al3-C3, and Al4-C3 bonds, are closed to one another, indicating similar bonding strengths against compression. The slight deviation may be due to different coordination environment of carbon atoms. With respect to the Al-C and Si-C bonds orienting along the basal plane, it is noticed that the contraction tendencies resemble those of Al2-C2, Al3-C3, and Al4-C3 bonds. The curves deviate the data of Al2-C2, Al3-C3, and Al4-C3 bonds in small magnitude. It is hard to distinguish these curves in the studied pressure range. This result shows similar bonding strength of the investigated bonds. For brevity, the bond-length contractions of bonds orienting along the basal plane are not plotted in Fig. 2.

As shown in the inset of Fig. 2, the c/a ratio decreases continuously as the pressure increases up to 50 GPa. The tendency demonstrates that c axis contracts more than a axis does in the pressure range examined. This indicates that Al_4SiC_4 is stiffer in the basal plane than that parallel to the $[0001]$ direction. Therefore, Al_4SiC_4 is anisotropic in elastic stiffness through the investigated pressures. Under each applied hydrostatic pressure, we optimized the crystal structure by relaxing the cell degrees of freedom with no constraint. Based on the monotonous behavior of those bond length contraction curves, no pressure-induced phase transition occurs in Al_4SiC_4 . Strong covalent bonding between Al-C and Si-C bonds in hexagonal lattice provide no phase transition.

Table II includes computed second-order elastic constants of Al_4SiC_4 , Al_4C_3 , and 4H-SiC . We note that the elastic constants of Al_4SiC_4 are more close to those of Al_4C_3 , but differ significantly from the corresponding values of 4H-SiC . The elastic constants c_{11} and c_{33} , which represent stiffness against principal strains, exhibit slightly higher values for Al_4SiC_4 compared with those of Al_4C_3 . The enhancements are attributed to the positive contribution of strong coupling between the Al_4C_3 - and SiC-type structural units in Al_4SiC_4 . The c_{44} and c_{66} , which are related to the shear resistance in the $\{100\}$ $\langle 110 \rangle$ and $\{010\}$ $\langle 001 \rangle$ directions, respectively, show higher values for Al_4SiC_4 with respect to those of Al_4C_3 as well. Mechanical parameters of polycrystalline, such as bulk modulus B and shear modulus G , are computed from the elastic coefficient tensor, and are listed in Table III. The computed bulk modulus B for Al_4SiC_4 is 179 GPa, and is in good agreement with the experimental data, 182 GPa, obtained by fitting the Birch-Murnaghan equation of state.¹³ Compared to those of Al_4C_3 , the bulk modulus B and shear modulus G of Al_4SiC_4 are enhanced by 9 and 11 GPa, respectively. Based on a close, but slightly higher, mechanical parameters of Al_4SiC_4 and Al_4C_3 , the Al_4C_3 -type structural units dominate the mechanical properties of Al_4SiC_4 , while, the other con-

TABLE III. Calculated ideal tensile σ and shear τ strengths (in GPa), bulk modulus B (in GPa), and shear modulus G (in GPa) of Al_4SiC_4 , Al_4C_3 , and 4H-SiC , together with the strain energy differences $\Delta E = E_t - E_s$ (in eV/formula), where E_t and E_s are strain energies at the maximum tensile and shear stresses, respectively.

Compound	B	G	σ	τ	ΔE
Al_4SiC_4	179	140	20	18	-0.415
Al_4C_3	170	129	21	22	-1.000
4H-SiC	226	209	48	38	-0.263

stituent unit in SiC-type arrangement and the strong coupling between each structural unit also play a role in enhancing the mechanical properties of Al_4SiC_4 .

IV. IDEAL STRENGTH AND ATOMISTIC DEFORMATION MODES

Material deformation is strain dependent and elastic parameters may not always give accurate account for all macroscopic mechanical properties, such as properties related to atomic plane slip. The reason can be attributed to the fact that these elastic parameters are computed under equilibrium conditions; while material deformation associated with experimental strengths occurs at strains where atomic bonding characteristics change significantly. Therefore, studies of the theoretical stress-strain relationships following a material strained from elasticity to the limit of its structural stability and the underlying atomistic deformation modes are important in understanding structural stability, strengths, hardness, and ductility.

In Fig. 3, we present the calculated Hellmann-Feynman stresses for Al_4SiC_4 at various tensile and shear strains, to

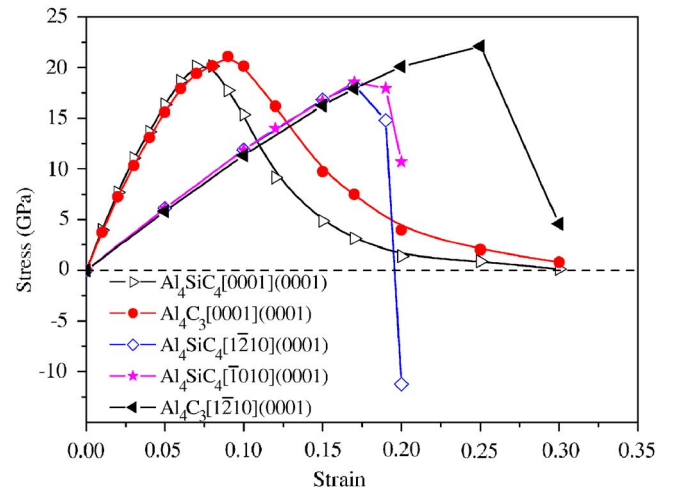


FIG. 3. (Color online) Calculated stress-strain relation for Al_4SiC_4 and Al_4C_3 . Solid circles and empty triangles represent tensile stresses along c direction for Al_4C_3 and Al_4SiC_4 , respectively; empty diamonds and solid pentagons correspond to the shear stresses of Al_4SiC_4 , for $[1\bar{2}10](0001)$ and $[1\bar{1}01](0001)$ slip systems, respectively; and the shear strain in $[1\bar{2}10](0001)$ direction is displayed by solid triangles for Al_4C_3 .

gether with the data of Al_4C_3 for comparison. The tensile strain was imposed along the high-symmetry $[0001]$ direction of hexagonal material. As the lattice constant c increases, the crystal is reconfigured to relax the lateral stresses. The calculated tensile stress-strain curves exhibit similar trends for Al_4SiC_4 and Al_4C_3 , except for larger critical strain sustained by Al_4C_3 before stress relaxation. The tensile strength of Al_4SiC_4 experienced a slightly lower value of 20 GPa, while, the tensile strength is 21 GPa for Al_4C_3 , as tabulated in Table III.

For compound with hexagonal symmetry with large c/a axis ratio, basal-plane slip can be activated in the $[\bar{1}210](0001)$ or $[\bar{1}010](0001)$ direction, depending on which direction is weak and more operative. To distinguish the slip system of Al_4SiC_4 with space group $P6_3mc$, we applied shear strain along the $[\bar{1}210](0001)$ and $[\bar{1}010](0001)$ direction and calculated the theoretical stress-strain relationship as shown in Fig. 3. It is noted that stress-strain curves for $[\bar{1}210](0001)$ and $[\bar{1}010](0001)$ shear strains are the same up to shear strain of 0.15. Maximum shear stress of Al_4SiC_4 achieves at strain of 0.17 simultaneously for the two shear deformation paths. The ideal shear strength for $[\bar{1}210](0001)$ shear deformation is only 0.3 GPa larger than that of the $[\bar{1}010](0001)$ shear mode. This suggests similar deformation mechanism for the two strain modes. Therefore, we only analyze atomistic deformation modes and electronic structure mechanism for $[\bar{1}210](0001)$ shear deformation in the present paper for brevity.

A comparison between Al_4SiC_4 and Al_4C_3 under $[\bar{1}210] \times (0001)$ shear strain shows resemblance in linear region but a dramatic difference at a large shear strain. Not only the critical strain sustained by Al_4SiC_4 differs from that by Al_4C_3 , but the stress softening beyond the critical strain are also obviously different for the two materials. Along the $[\bar{1}210](0001)$ shear path for Al_4SiC_4 , the stress approaches maximum value at a strain around 0.19 and drops abruptly thereafter, suggesting sudden bond-breaking events at large shear strain. The Al_4C_3 lattice sustains larger critical shear deformation on the other hand, and the critical shear strain achieves 0.25. The distinguishable stress-strain curve raises a suspicion that shear-induced structural instability should be different for Al_4SiC_4 and Al_4C_3 under applied $[\bar{1}210] \times (0001)$ shear strain. Due to the less sustained critical strain, the ideal shear strength of Al_4SiC_4 is 4 GPa smaller than that of binary carbide Al_4C_3 , which are 18 GPa and 22 GPa, respectively.

It is noticeable in Fig. 3 that bond softening occurs earlier under tensile strain, compared to the case of under shear strain. Hence it is of interest to distinguish the two atomistic deformation modes, i.e., tension and shear, because the stress-strain curves yield obviously different tendency. A tension-induced lattice failure would probably result in cleavage, whereas a shear-induced instability may homogeneously nucleate defects, such as dislocation. The failure mode of a material depends on which type of lattice instability being encountered first. The ideal strength, i.e., the stress at which a perfect crystal becomes mechanically unstable,

corresponds to the inflexion point along energy surface with respect to the applied strain. The knowledge of strain energy at the maximum stress may provide insights into the mechanism of preferred failure modes. With the calculated strain energy, one can evaluate the competition between the tensile and shear deformation modes, and thus predict either ductile or brittle response of a solid is allowed.³² In our previous works,²² we have revealed that for brittle binary ceramic as TiC, the ratio of ideal tensile to shear strength is nearly unitary. By comparing the strain energies, at which the maximum tensile and shear stress are achieved, we obtained that tensile strain energy was well below the shear strain energy by 0.058 eV/formula for TiC crystal, implying cleavage may intrude prior to shear instability. In contrast, the strain energies corresponding to ideal tensile strength have higher values by 0.740 and 0.695 eV/formula, respectively, than the shear energies for Ti_2AlC and Ti_2AlN , which are machinable ceramics capable of damage tolerance and intrinsic toughness. These results indicate that the shear-induced failure is more energetically favorable and can be reached first upon loading for these two compounds. Based on the same idea, we performed calculations on Al_4SiC_4 , Al_4C_3 , and 4H-SiC in the present work, and the tensile strain energies corresponding to critical tensile stresses are determined to be 0.415, 1.000, and 0.263 eV/formula smaller than the shear strain energies at each critical shear stress, respectively, as tabulated in Table III. Therefore, Al_4SiC_4 is most likely to fail in tension and hence, suggested cleavage fracture mechanism and intrinsic brittleness. Suppose a perfect crystal is deformed theoretically, one can assess the competition between the uniaxial tension and shear stresses by resolving the stress onto the slip systems and comparing with the ideal strengths. Although ideal shear strength is slightly lower than the tensile strength, by resolving the tensile stress onto the slip systems, the resulting shear stress may be much lower than the ideal shear strength. Therefore, the material is expected to fail by tension. Moreover, it is interesting to note that the

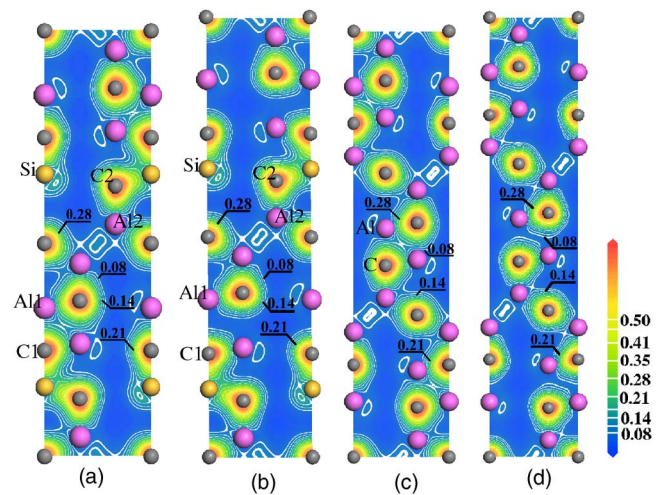


FIG. 4. (Color online) Valence electron density of a slice of the $(11\bar{2}0)$ plane for unstrained Al_4SiC_4 is shown in (a); whereas (b) corresponds to the case under applied tensile strain of 0.1 along the c direction. The (c) and (d) figures are similar to (a) and (b) except for Al_4C_3 . The contour lines range from 0.00 to 0.78 electron/ \AA^3 .

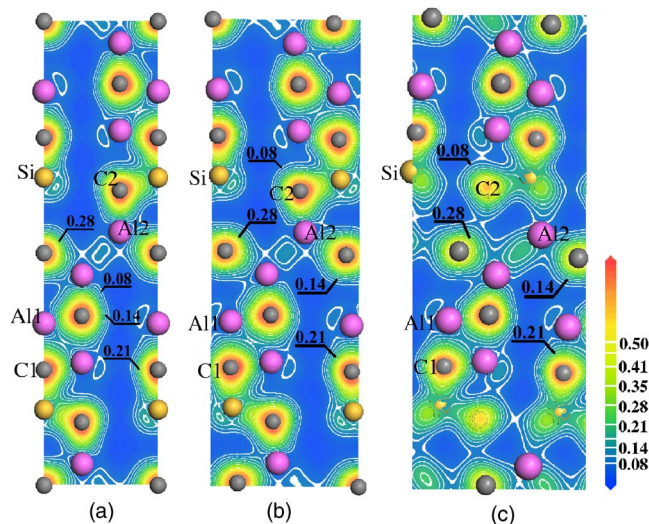


FIG. 5. (Color online) Valence electron density of a slice of the $(11\bar{2}0)$ plane in Al_4SiC_4 unit cell under shear deformations of (a) $\varepsilon=0$, (b) $\varepsilon=0.1$, and (c) $\varepsilon=0.2$. The contour lines range from 0.00 to 0.78 electron/ \AA^3 .

stress of Al_4SiC_4 drops abruptly beyond the critical strain. Such behavior has been frequently experienced by hard or brittle ceramics, such as diamond and *c*-BN.³³

To further understand the deformation processes at various strains, it is helpful to examine the charge density contours. In Fig. 4, charge density contours of unstrained Al_4SiC_4 and Al_4C_3 crystals and those under applied tensile strain of 0.1 are illustrated for a slice of $(11\bar{2}0)$ plane. Upon tensile loading, bond-breaking events are indicated by charge depletions from the stretched Al-C bonds, i.e., Al1-C1 bond in Al_4SiC_4 . This leads to the structural failure of both crystalline at small strains. Because bond breaking occurs inside the Al_4C_3 -type units in Al_4SiC_4 , it is likely that Al_4SiC_4 and Al_4C_3 will show similar mechanical properties that are determined by tension-induced structural instability. In other words, the cleavage of Al_4SiC_4 may be originated from the bond-breaking inside the Al_4C_3 -type unit.

In contrast, the structural failure upon shear strain exhibits different atomistic deformation mechanism for Al_4SiC_4 , as shown in Fig. 5. The softening and breaking of the Al2-C2 bond, instead of the weakest Al1-C1 bond, lead to the structural instability of Al_4SiC_4 under shear deformation. Particularly, the Al2-C2 bond corresponds to the coupling between

Al_4C_3 - and SiC-type structural units. According to previous investigation, we know that the *p* orbital involved covalent bond may behave diversely in response to tension or shear strain.²² The extensively distributed *p* states of Al-C covalent bond is expected to respond more readily to the shear deformation than to tension. Therefore, a slightly lower shear strength of Al_4SiC_4 is obtained compared with tensile strength, despite stronger Al2-C2 bond is involved in shear-induced instability.

V. CONCLUSIONS

In summary, we investigated the bonding characteristics, elastic stiffness, ideal strengths, and atomistic deformation modes of Al_4SiC_4 by first-principles calculations. We show that the mechanical properties are closely related to the crystal structure of Al_4SiC_4 , which could be described as Al_4C_3 -type structural units and hexagonal SiC-type units stacked along $[0001]$ direction. The elastic moduli of Al_4SiC_4 show more resemblance to its binary counterpart, Al_4C_3 . Bonding strengths analysis of Al_4SiC_4 under various hydrostatic pressures demonstrated a strong coupling between the Al_4C_3 - and SiC-type structural units. Bond-softening and bond-breaking processes upon tensile and shear deformations were illustrated and compared for Al_4SiC_4 and Al_4C_3 . The results show how interatomic bonds in the ternary carbide respond to applied strains, especially strain near structural instability. Tension-induced bond-breaking occurs inside the constitutive Al_4C_3 -type structural unit, which provides Al_4SiC_4 a similar tensile strength with Al_4C_3 . On the other hand, shear-induced instability is originated from the coupling bond between Al_4C_3 - and SiC-type structural units. In addition, the lower strain energy at maximum tensile stress, i.e. ideal strength, than the energies in shear cases, together with deformation modes, suggest cleavage fracture mechanism and an intrinsic brittle character of Al_4SiC_4 . To better understand the mechanical properties of a material with alternatively stacked structural units, one can trace back to the properties of each constituent structural unit and the coupling strength between them. Both may play a key role in determining the inherent mechanical properties.

ACKNOWLEDGMENTS

This work was supported by the National Outstanding Young Scientist Foundation for Y. C. Zhou under Grant No. 59925208 and by Natural Sciences Foundation of China under Grant Nos. 50232040, 90403027 and 50302011.

¹J. F. Huang, X. R. Zeng, H. J. Li, X. B. Xiong, and M. Huang, *Mater. Lett.* **58**, 2627 (2004).

²M. W. Barsoum, *Prog. Solid State Chem.* **28**, 201 (2000).

³J. C. Schuster and H. Nowotny, *Z. Metallkd.* **71**, 341 (1980).

⁴J. Y. Wang, Y. C. Zhou, Z. J. Lin, T. Liao, and L. F. He, *Phys. Rev. B* **73**, 134107 (2006).

⁵T. M. Gesing and W. Jeitschko, *J. Solid State Chem.* **140**, 396 (1998).

⁶S. E. Lofland, J. D. Hettinger, K. Harrell, P. Finkel, S. Gupta, M. W. Barsoum, and G. Hug, *Appl. Phys. Lett.* **84**, 508 (2004).

⁷Z. M. Sun, D. Music, R. Ahuja, and J. M. Schneider, *J. Phys.: Condens. Matter* **17**, L15 (2005).

⁸J. Y. Wang and Y. C. Zhou, *J. Phys.: Condens. Matter* **16**, 2819 (2004).

⁹K. Inoue, S. Mori, and A. Yamaguchi, *J. Ceram. Soc. Jpn.* **111**, 348 (2003).

- ¹⁰K. Inoue, S. Mori, and A. Yamaguchi, *J. Ceram. Soc. Jpn.* **111**, 126 (2003).
- ¹¹O. Yamamoto, M. Ohtani, and T. Sasamoto, *J. Mater. Res.* **17**, 774 (2002).
- ¹²K. Inoue, A. Yamaguchi, and S. Hashimoto, *J. Ceram. Soc. Jpn.* **110**, 1010 (2002).
- ¹³V. L. Solozhenko and O. O. Kurakevych, *Solid State Commun.* **135**, 87 (2005).
- ¹⁴S. H. Jhi, J. Ihm, S. G. Louie, and M. L. Cohen, *Science* **399**, 132 (1999).
- ¹⁵D. Roundy, C. R. Krenn, M. L. Cohen, and J. W. Morris, *Phys. Rev. Lett.* **82**, 2713 (1999).
- ¹⁶S. Ogata, J. Li, N. Hirotsaki, Y. Shibutani, and S. Yip, *Phys. Rev. B* **70**, 104104 (2004).
- ¹⁷M. Jahnátek, M. Krajčí, and J. Hafner, *Phys. Rev. B* **71**, 024101 (2005).
- ¹⁸D. M. Clatterbuck, D. C. Chrzan, and J. W. Morris, *Acta Mater.* **51**, 2271 (2003).
- ¹⁹J. Frenkel, *Z. Phys.* **37**, 572 (1926).
- ²⁰J. H. Rose, J. R. Smith, and J. Ferrante, *Phys. Rev. B* **28**, 1835 (1983).
- ²¹G. Xu, A. S. Argon, and M. Ortiz, *Philos. Mag. A* **72**, 415 (1995).
- ²²T. Liao, J. Y. Wang, and Y. C. Zhou, *Phys. Rev. B* **73**, 214109 (2006).
- ²³M. D. Segall, P. L. D. Lindan, M. J. Probert, C. J. Pickard, P. J. Hasnip, S. J. Clark, and M. C. Payne, *J. Phys.: Condens. Matter* **14**, 2717 (2002).
- ²⁴D. Vanderbilt, *Phys. Rev. B* **41**, 7892 (1990).
- ²⁵J. P. Perdew, J. A. Chevary, S. H. Vosko, K. A. Jackson, M. R. Pederson, D. J. Singh, and C. Fiolhais, *Phys. Rev. B* **46**, 6671 (1992).
- ²⁶J. D. Pack and H. J. Monkhorst, *Phys. Rev. B* **16**, 1748 (1977).
- ²⁷B. G. Pfrommer, M. Côté, S. G. Louie, and M. L. Cohen, *J. Comp. Physiol.* **131**, 233 (1997).
- ²⁸V. Milman and M. C. Warren, *J. Phys.: Condens. Matter* **13**, 241 (2001).
- ²⁹P. Ravindran, L. Fast, P. A. Korzhavyi, B. Johansson, J. Wills, and O. Eriksson, *J. Appl. Phys.* **84**, 4891 (1998).
- ³⁰Powder Diffraction File, No. 11-629, Joint Committee on Powder Diffraction Standards, Swarthmore, Pennsylvania (1972).
- ³¹A. Bauer, J. Krausslich, L. Dressler, P. Kuschnerus, J. Wolf, K. Goetz, P. Kackell, J. Furthmuller, and F. Bechstedt, *Phys. Rev. B* **57**, 2647 (1998).
- ³²A. Kelly, *Strong Solids* (Oxford University Press, London, 1966).
- ³³Y. Zhang, H. Sun, and C. F. Chen, *Phys. Rev. Lett.* **94**, 145505 (2005).